Bioactive Materials 29 (2023) 241–250

Contents lists available at ScienceDirect

Bioactive Materials

journal homepage: www.keaipublishing.com/en/journals/bioactive-materials

# Addition of heparin binding sites strongly increases the bone forming capabilities of BMP9 *in vivo*

Claudia Siverino [a,2,3], Shorouk Fahmy-Garcia [b,c,d,2,1], Viktoria Niklaus [a], Nicole Kops [b], Laura Dolcini [e], Massimiliano Maraglino Misciagna [e], Yanto Ridwan [f], Eric Farrell [d,*], Gerjo J.V.M. van Osch [b,g,h], Joachim Nickel [a,i,**]

[a] Department of Tissue Engineering and Regenerative Medicine, University Hospital Wuerzburg, Wuerzburg, Germany
[b] Department of Orthopaedics and Sports Medicine, Erasmus MC, University Medical Center, Rotterdam, the Netherlands
[c] Department of Internal Medicine, Erasmus MC, University Medical Center, Rotterdam, the Netherlands
[d] Department of Oral and Maxillofacial Surgery, Erasmus MC, University Medical Center, Rotterdam, the Netherlands
[e] Fin-Ceramica Faenza SpA, Via Granarolo 177/3, 48018, Faenza, Italy
[f] AMIE Core Facility, Erasmus University Medical Center, Rotterdam, the Netherlands
[g] Department of Otorhinolaryngology, Head and Neck Surgery, Erasmus MC, University Medical Center, Rotterdam, the Netherlands
[h] Department of Biomechanical Engineering, Faculty of Mechanical, Maritime and Materials Engineering, Delft University of Technology, Delft, the Netherlands
[i] Fraunhofer ISC, Translational Center RT, Wuerzburg, Germany

ARTICLE INFO

*Keywords:*
Bone morphogenetic protein 9 (BMP9)
Heparin binding sites
Bone regeneration
Subcutaneous animal model

ABSTRACT

Bone Morphogenetic proteins (BMPs) like BMP2 and BMP7 have shown great potential in the treatment of severe bone defects. In recent *in vitro* studies, BMP9 revealed the highest osteogenic potential compared to other BMPs, possibly due to its unique signaling pathways that differs from other osteogenic BMPs. However, *in vivo* the bone forming capacity of BMP9-adsorbed scaffolds is not superior to BMP2 or BMP7. *In silico* analysis of the BMP9 protein sequence revealed that BMP9, in contrast to other osteogenic BMPs such as BMP2, completely lacks so-called heparin binding motifs that enable extracellular matrix (ECM) interactions which in general might be essential for the BMPs' osteogenic function. Therefore, we genetically engineered a new BMP9 variant by adding BMP2-derived heparin binding motifs to the N-terminal segment of BMP9's mature part. The resulting protein (BMP9 HB) showed higher heparin binding affinity than BMP2, similar osteogenic activity *in vitro* and comparable binding affinities to BMPR-II and ALK1 compared to BMP9. However, remarkable differences were observed when BMP9 HB was adsorbed to collagen scaffolds and implanted subcutaneously in the dorsum of rats, showing a consistent and significant increase in bone volume and density compared to BMP2 and BMP9. Even at 10-fold lower BMP9 HB doses bone tissue formation was observed. This innovative approach of significantly enhancing the osteogenic properties of BMP9 simply by addition of ECM binding motifs, could constitute a valuable replacement to the commonly used BMPs. The possibility to use lower protein doses demonstrates BMP9 HB's high translational potential.

## 1. Introduction

The principle of bone formation by autoinduction as first described by Marshall Urist has started pioneering approaches which revolutionized therapies in the field of skeletal malfunctions including non-union bone fractures as well as osteopenia or osteoporosis [1]. After the identification of the proteins, which initiate this bone forming process, the so-called Bone Morphogenetic Proteins (BMPs), various investigations were started to understand the underlying molecular mechanisms but also to establish procedures for clinical use. To date,

* Corresponding author. Dr Molewaterplein 40, 3015GD Rotterdam, the Netherlands.
** Corresponding author. Röntgenring 11, 97070 Würzburg, Germany.
*E-mail addresses:* e.farrell@erasmusmc.nl (E. Farrell), joachim.nickel@uni-wuerzburg.de (J. Nickel).
[1] Fahmy-Garcia current address: Janssen Vaccines & Prevention B.V, The Netherlands.
[2] the authors contributed equally to the work.
[3] Siverino current address: AO Research Institute Davos Platz, Switzerland.

https://doi.org/10.1016/j.bioactmat.2023.07.010
Received 9 March 2023; Received in revised form 29 June 2023; Accepted 9 July 2023
Available online 18 July 2023

BMP2 and BMP7 have received FDA approval and subsequently have been used to treat tibial non-unions, for craniomaxillofacial reconstructions and for single level anterior lumbar interbody fusion (ALIF) [2–5]. However, several studies reported that the use of BMP2 or BMP7 in humans often caused a variety of severe side effects such as local erythema, swelling, heterotopic ossification, postoperative radiculitis, postoperative nerve root injury, and others [6,7]. These side effects are most-likely connected to the supraphysiological doses which are needed to induce the osteogenic responses in those cells being involved in the bone forming process [8].

The commonly used growth factor delivery methods focus on non-covalent techniques such as adsorption to – and/or encapsulation within innovative scaffold materials [9]. However, delivery of adsorbed growth factors often results in an initial burst release. This causes the necessity to use higher doses to compensate for the loss of the released protein which, due to diffusion, is no longer available at the implantation site. Another strategy involves the modification of the growth factor (i.e., BMP2) to ensure a more stable and specific connection to the used scaffold material, such as the insertion of specific binding motifs or affinity tags at the N-terminus of BMP2 that has shown maintained bioactivity of the immobilized protein *in vitro* [10–14].

A method to increase BMP2 entrapment was suggested from Würzler et al. by adding extra heparin binding sites to the already existing ones at the N-terminus of wild type BMP2 (BMP2 WT) [15,16]. The addition of the extra heparin binding sites increases the binding to extracellular matrix (ECM) structures [17] thus allowing a stronger entrapment of the growth factor within the ECM which consequently lowers its diffusibility. This results in a prolonged retention time of the growth factor at the implantation site. Implantation of these variants (named T3-or T4-BMP2) into the hind limb muscle of rats resulted in increased bone formation compared to implantation of BMP2 WT. In general, approaches focusing either on better delivery strategies or the enhancement of the growth factor's capabilities to induce bone formation as described above aim to improve clinical applications in terms of safety aspects and the reduction of costs e.g., by reducing the required growth factor doses.

In 2003 the osteogenic potential of 14 different BMP members was investigated [18]. Surprisingly, among the 14 BMPs, BMP9 revealed the highest osteogenic potential in C2C12 cells which were transduced with the corresponding BMP-encoding adenoviral expression vectors. BMP9 induced the highest expression levels of alkaline phosphatase (ALP) *in vitro* and moreover induced greater ectopic bone formation upon implantation of these modified cells into animals [18,19].

*In vivo* BMP9 is highly expressed in the developing mouse liver and stimulates hepatocyte proliferation [20]. It also induces and maintains the cholinergic phenotype within basal forebrain neurons, inhibits hepatic glucose production, inhibits critical enzymes of lipid metabolism, and helps to maintain the homeostasis of iron metabolism [21]. BMP9 is also a synergistic factor in hematopoietic progenitor cell generation [22]. Various *Bmp* null knockouts, such as *Bmp2*, *Bmp4* and *Bmp7* result in embryonic lethality, showing the importance of these factors already in early embryonal development. Additionally, conditional knock-out scenarios demonstrated, that the deletion of BMP2 expression in adult mice strongly affects endochondral fracture healing due to an impaired callus formation [23] implicating an important role of BMP2 in early stages of bone formation. Instead, *Bmp9* null knockout mice are viable and fertile and, importantly, do not show compromising effects on the bone phenotype [24,25]. Moreover, in contrast to other BMPs (i.e., BMP2, BMP6, and BMP7), BMP9 signals via and binds with high binding affinity to another type I receptor, the activin-like kinase receptor (ALK)1 and does not bind to the BMP type I receptor BMPR-IA (ALK3) [26]. Furthermore, expressing dominant-negative (dn) ALK1 receptor variants in osteogenic precursors cell lines, such as C3H10T1/2 or C2C12 resulted in a strong inhibition of osteogenic differentiation, suggesting that the mechanisms governing BMP9-mediated osteoinduction may differ from the other osteogenic BMPs [19,21,22,27,28]. Even if BMP9 appears not to be fundamental for embryonal bone development and it acts by binding to different receptors than the other osteogenic proteins, it has shown strong osteogenic potential *in vitro* and *in vivo* when implanting adenovirus-transduced cells into animals [19].

To date, only a few *in vivo* studies have been performed using scaffolds loaded with recombinant human (rh) BMP9 in different animal models. Robust bone formation induced by the recombinant protein was observed in calvaria defect models indicating that rhBMP9 can trigger ossification [29,30]. However, one study also reports osteoinduction by ectopically applied rhBMP9 in muscle tissue [30].

*In silico* analysis of the BMP9 sequence revealed that BMP9, in contrast to other osteogenic BMPs such as BMP2, lacks the so-called heparin binding motifs enabling ECM interactions [27]. As these motifs enable the ligand's entrapment within ECM structures we assume, that without these motifs an otherwise strong osteogenic BMP may act only poorly due to its high diffusibility.

For this purpose, a BMP9 variant (BMP9 HB) was constructed by fusing the heparin binding sites located in the N-terminal segment of BMP2 with the cysteine-knot motif containing BMP9 C-terminus. The bioactivity of the resulting chimera was directly compared with that of BMP2 WT and BMP9 WT in terms of receptor binding *in vitro* and its osteogenic potential in cell-based assays as well as in animal experiments.

## 2. Results

### 2.1. BMP9 HB and BMP9 WT show similar bioactivities in vitro

The new BMP9 HB has, as expected, a little higher molecular weight compared to BMP9 WT (~13 kDa and ~12 kDa under reducing and ~26 kDa and ~24 kDa under non-reducing conditions, respectively) as analyzed by SDS-PAGE and Coomassie Brilliant Blue staining (Fig. 1 A). BMP9 HB and BMP9 WT both induced higher levels of alkaline phosphatase (ALP) enzymatic activity with lower $EC_{50}$ values (BMP9 WT: 0.87 nM and BMP9 HB: 2.4 nM) compared to BMP2 WT (22 nM) (Fig. 1 B). Binding of the different ligands to heparin was analyzed by surface plasmon resonance (SPR). Significant binding to heparin was only observed in case of ligands which contain heparin binding sites (i.e., BMP9 HB and BMP2 WT) whereas under identical conditions BMP9 WT and an enzymatically cleaved BMP2 variant, called "coreBMP2" just bound very weakly to the heparin coated sensor chip. The data concerning coreBMP2s' bioactivity have been already reported by Heinecke et al. [31]. Fitting recorded sensorgrams to a 1:1 Langmuir binding model result in apparent $K_D$ values of 23.9 nM ± 9.3 nM for the BMP9 HB and 186 nM ± 32.9 nM for the BMP2 WT:heparin interaction. Noteworthy, the binding kinetics of BMP9 HB and BMP2 WT differ significantly (Fig. 1C). SPR analyses of ligand:receptor interactions showed that in contrast to BMP2 WT, which binds strongly to the extracellular domain (ECD) of BMPR-IA ($K_D$: 2.53 nM ± 1.3 nM) binding of BMP9 HB to this receptor ECD could not be observed (Fig. 1 D, BMPR-$IA_{ECD}$). Also, BMP9 WT did not bind to BMPR-IA (data not shown) in agreement with published data [32]. In order to directly compare the binding characteristics of BMP9 WT and BMP9 HB, binding of both ligands to BMPR-$II_{ECD}$ was analyzed and compared with that of BMP2 WT (Fig. 1 D, BMPR-$II_{ECD}$). Recorded sensorgrams of BMP9 HB:BMPR-$II_{ECD}$- and BMP9 WT:BMPR-$II_{ECD}$ interactions are highly similar with calculated apparent $K_D$ values of 11.6 nM ± 5.3 nM for the BMP9 HB: BMPR-$II_{ECD}$- and 13.3 nM ± 3.8 nM for the BMP9 WT:BMPR-$II_{ECD}$ interaction. The evaluated binding affinity of BMP2 WT to this receptor ECD is 66.9 nM ± 22.5 nM which is also in agreement with values reported earlier [31]. Also binding of BMP9 HB and BMP9 WT to $ALK1_{ECD}$ is almost identical with apparent $K_D$ values of 5.59 nM ± 2.49 nM for the BMP9 HB:$ALK1_{ECD}$- and 4.76 nM ± 1.29 nM for the BMP9 WT:$ALK1_{ECD}$ interaction (Fig. 1 E). Both, BMP2 WT and coreBMP2 do not bind to $ALK1_{ECD}$ (Fig. 1 E).

As known the signaling of BMPs can be triggered by a variety of

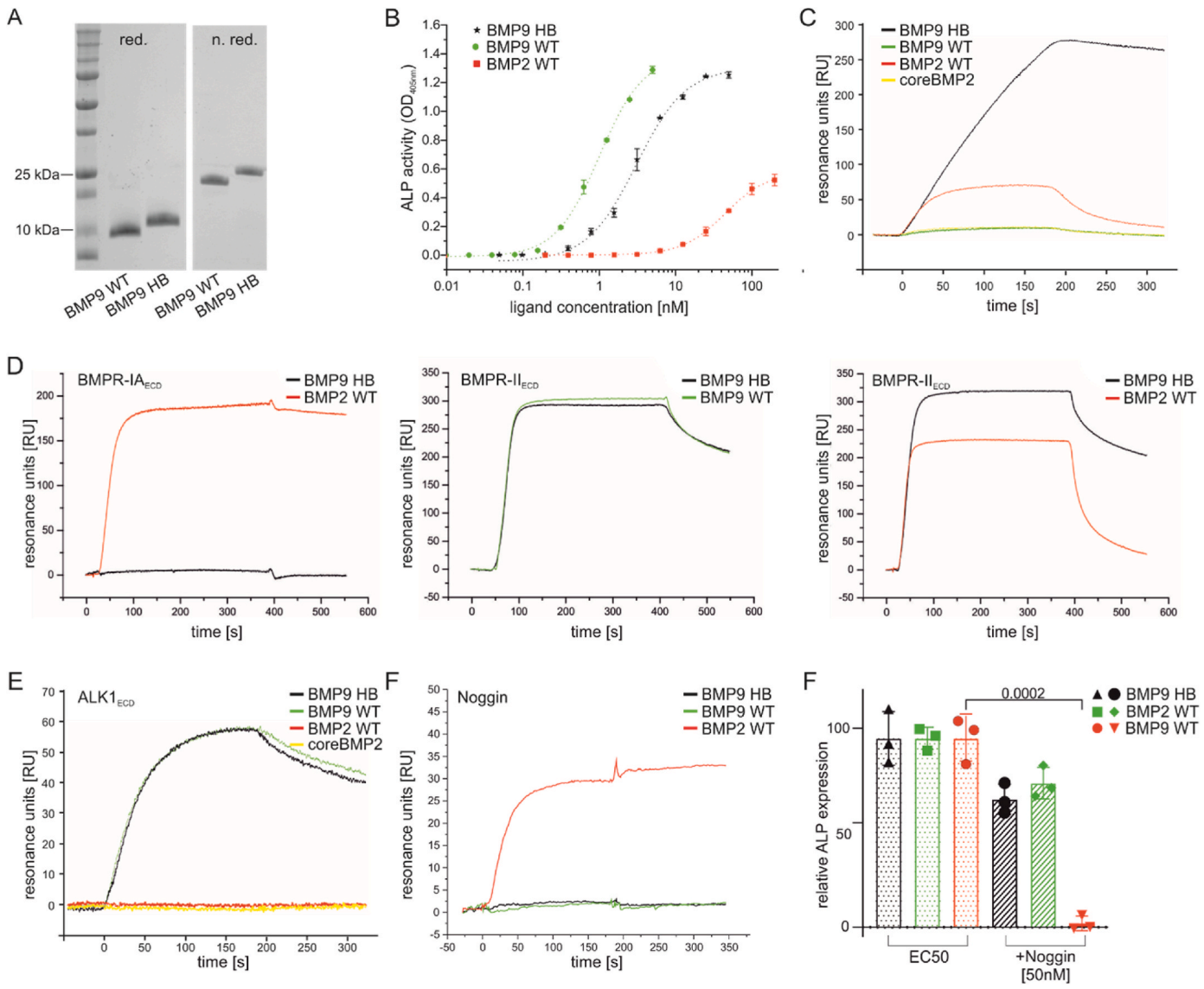


**Fig. 1.** Biological activities of BMP9 HB compared to the BMP2 WT and BMP9 WT. (A) Coomassie Brilliant Blue staining of BMP9 WT and BMP9 HB separated by SDS-PAGE under reducing and non-reducing conditions; (B) Dose-dependent ALP activity in C2C12 cells induced by the indicated ligands. The calculated $EC_{50}$ values are: BMP9 WT: 0.87 nM ± 0.21 nM, BMP9 HB: 2.4 nM ± 0.85 nM and BMP2 WT 22 nM ± 9.3 nM). The background absorption (without ligand, $OD_{405nm}$: 0.045) was subtracted from all recorded values. (C) Selected surface plasmon resonance (SPR) sensorgrams depict the interactions of the indicated ligands with heparin at 200 nM ligand concentration. Selected SPR sensorgrams depict the interactions of the indicated ligands with (D) $BMPR\text{-}IA_{ECD}$ or $BMPR\text{-}II_{ECD}$ or (E) with $ALK1_{ECD}$ at 200 nM ligand concentration and (F) with Noggin at 62.5 nM ligand concentration. Apparent $K_D$ values (presented in text) were calculated as described in the material and methods section. (G) ALP activity in C2C12 cells was induced by the indicated ligands at concentration reflecting their individual $EC_{50}$ values with or without the presence of 50 nM Noggin.

factors acting either in the extracellular space, but also at the level of the cell membrane and in the cytosol [33,34]. Interactions with the modulator protein Noggin are of special interest since a "Noggin insensitivity" for BMP9 WT to this modulator has been reported [35]. We therefore also analyzed the binding of BMP9 WT and BMP9 HB to immobilized Noggin and compared binding capabilities with those of BMP2 WT (Fig. 1 F). In contrast to BMP2 WT which binds strongly to Noggin (apparent $K_D$ value: 1.2 nM ± 0.7 nM) neither BMP9 WT nor BMP9 HB interact with Noggin, even at the highest concentrations tested (200 nM). Interestingly, the kinetic rate constants for the BMP2: Noggin interaction could not be evaluated due to very low dissociation rates ($k_{off}$). Therefore, the $K_D$ values for this interaction are determined by dose dependent equilibrium binding using at least 6 different ligand concentrations. The obtained values are in agreement with data already published [36]. The reported Noggin insensitivity could also be confirmed for BMP9 HB *in vitro*. In our standard ALP test only BMP2 WT-induced ALP activity was significantly inhibited ($p = 0.0002$) by parallel application of Noggin, while BMP9 HB and BMP9 WT were only mildly affected by Noggin (Fig. 1 G).

To test whether glycosylation is also important for BMP9-mediated signal transduction, we analyzed the potential presence of sugar moieties in BMP9 WT (CHO-cell derived) compared to BMP9 HB (*E.coli* derived) (Suppl. Fig. 1). Both proteins lack so-called N-linked glycosylation sites (NXS/T), but O-glycosylation might be present at least in the CHO-derived BMP9 WT protein. A direct comparison of the individual staining intensities demonstrates that only the positive control is strongly stained, whereas the negative control and both, BMP9 HB and BMP9 WT are only weakly stained, comparable to the provided negative control (Suppl. Fig. 1).

### 2.2. BMP9 HB is released more slowly from the collagen scaffold than BMP9 WT

The collagen scaffold was characterized by Scanning Electron Microscopy (SEM) (Fig. 2 A). The release profiles of BMP9 HB from the collagen scaffold were compared to those obtained for BMP9 WT (Fig. 2 B). In both cases, a burst release was observed within the first 24 h reaching a plateau after 48 h. The amount of BMP9 HB being released from the collagen scaffold after 7 days was, however, approximately 90 times lower than that of BMP9 WT (Fig. 2B). The release of BMP9 HB was similar to the release profile of BMP2 WT (Suppl. Fig. 2).

### 2.3. Low doses of BMP9 HB show bone formation already 3 weeks post implantation

Early phases of bone formation initiated by 1 μg or 10 μg of either BMP9 HB or BMP9 WT were investigated 3 weeks post implantation. BMP2 WT was not included as a condition since previous studies were already performed with both doses of BMP2 WT and evaluated at earlier time points by histology [37,38]. BMP9 HB at 1 μg induced bone formation with several dispersed bone areas observed in the outer part of the scaffold (Fig. 3 A, a). Remnants of the collagen scaffold were visible by histology. Implants loaded with 1 μg of BMP9 WT did not induce ectopic bone formation. Remnants of the collagen scaffold with some surrounding blood vessels were also present under these conditions (Fig. 3 B). At doses of 10 μg per implant both, BMP9 HB and BMP9 WT induced bone formation (Fig. 3C and D). Bone formation induced by 10 μg of BMP9 HB was present in the outer and center part of the collagen scaffold (Fig. 3C, c), while with BMP9 WT bone formation was more prevalent at the outer part of the scaffold (Fig. 3 D). Representative images of the implants using H&E staining are available in Suppl. Fig. 3.

### 2.4. BMP9 HB show different bone forming kinetics compared to BMP2 WT and BMP9 WT

Following on from the previous experiment we examined the kinetics of bone formation over time compared to BMP2 WT. The progression of mineralization was analyzed by microCT by *in vivo* longitudinal imaging at 3, 6, and 8 weeks, respectively (Fig. 4). The table below to the graph shows the number of subcutaneous mineralized tissues detected over a $n = 6$. Values different from 0 were scored as bone inducing implants. At 3 weeks post implantation (Fig. 4 A and D), most of the calcified tissue was observed for the 10 μg BMP2 WT cohort (6/6) followed by the 10 μg BMP9 HB group (5/6) and the least in the BMP9 WT 10 μg (3/6). At 1 μg, only implants loaded with BMP9 HB and BMP2 WT showed some calcification (2/6 and 1/6, respectively). Surprisingly, 6 weeks post implantation (Fig. 4 B and E), a notable increase in mineralized tissue was observed in BMP9 HB implants at both doses. The 10 μg BMP9 WT group also showed an increase at 6 weeks compared to the 3 weeks' time point. The 10 μg BMP2 WT group showed steady mineralized tissue from three weeks onwards. At 8 weeks post implantation (Fig. 4C and F) the 1 μg BMP9 HB group showed higher differences in both, bone volume and bone density (6/6) compared to the BMP2 WT (1/6) and BMP9 WT (2/6) at the same dose. At 10 μg all tested ligands produced comparable amounts of calcified tissue. Interestingly, the bone density induced by 10 μg of BMP2 WT was significantly higher compared to that induced by BMP9 WT or BMP9 HB. A table with the different conditions and implants which induced bone formation is available in the supplemental Fig. section (Suppl. Table 1).

### 2.5. Implants loaded with low doses of BMP9 HB display increased bone formation properties compared to those with the same amounts of the native BMPs

Retrieved implants were also scanned *ex vivo* at 8 weeks, thus allowing longer scan times resulting in finer resolutions (Fig. 5 A). Indeed, some of the implants that were not detected during the *in vivo* scanning, as shown in the graphs in Fig. 4, could now be included in the analyses.

To increase the power, a second batch of animals ($n = 4$ additional in 1 μg and 10 μg BMP9 HB and 10 μg BMP9) was operated and included in the mentioned groups. Additionally, a group with 0.1 μg BMP9 HB was added to the study.

The results confirmed the higher bone volume at 8 weeks of the ossicles induced by 1 μg BMP9 HB (10 implants formed detectable bones from $n = 10$) than that induced by the same dose of BMP2 WT (1 out of 6) or BMP9 WT (1 out of 6) (Fig. 5 A) and the absence of differences between the factors when added at a dose of 10 μg. Instead in case of 0.1 μg BMP9 HB, microCT scans did not show any bone mineralization after 8 weeks from implantation (0/6). Only 1/6 implants with 0.1 μg BMP9 HB could be retrieved and histological examination showed the presence of small parts of bone-like tissue, even though this was not detected on the *ex vivo* microCT scans (Fig. 5 B). The new bone was formed within the outer area of the collagen scaffold (Fig. 5 Bi, Bii) and collagen scaffold remnants were also observed (Fig. 5 Bi, Bii).

The 1 μg BMP9 HB loaded scaffolds induced bone formation resembling a long bone structure with the cortical area and blood vessels and fat tissue scattered in the central part similar to the structures observed in the bone marrow (Fig. 5C, Suppl. Fig. 4 A). Importantly, all 1 μg BMP9 HB-loaded scaffolds induced bone formation at significant levels (10/10 implants, details in Suppl. Table 1). The 1 μg BMP9 WT-loaded scaffold induced bone formation in small clusters with less than 100 μm size of bone tissue and only in 1 out of 6 implants (Fig. 5 D, Suppl. Fig. 4 B). BMP2 WT-loaded scaffold induced bone formation throughout the entire scaffold with fatty bone marrow and blood vessels (Fig. 5 E, Suppl. Fig. 4C) but only in 2 out of 6 implants (Fig. 5 E). Additionally, the scaffolds loaded with 1 μg doses showed remarkable size differences among the three ligands which is easily appreciable also from histology and in agreement with the microCT quantification shown before.

At 10 μg all tested ligands showed formation of new bone (Fig. 5 F, G and H) and in all the implants. Interestingly, the structure of the formed bone appeared different; BMP9 HB-loaded scaffold induced a denser bone shell at the outer part of the scaffold indicated by the intense red staining from the Masson's trichrome (Fig. 5 F). Similarly, with BMP9 WT the presence of bone tissue was more abundant at outer parts of the implant, but less compared to the BMP9 HB. Collagen remnants of the scaffold were observed only in the center of the implants, independent of

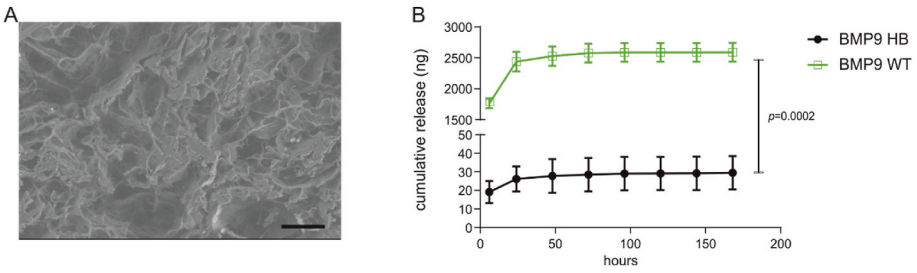


**Fig. 2.** *In vitro* BMP9 WT and BMP9 HB release. (A) SEM of the collagen scaffold processed in 1 wt% 1,4-butanediol di-glycidyl ether bis-epoxy carbonate (BDDGE) buffer at room temperature. Scale bar 100 μm (B) The cumulative release of BMP9 WT (green) and BMP9 HB (black) in alpha MEM with 1% Fungizone/gentamicin detected by ELISA is demonstrated over 7 days. Data represent mean values ± Standard Error of Mean. Statistical significance was validated by a non-parametric test, $p = 0.0002$.

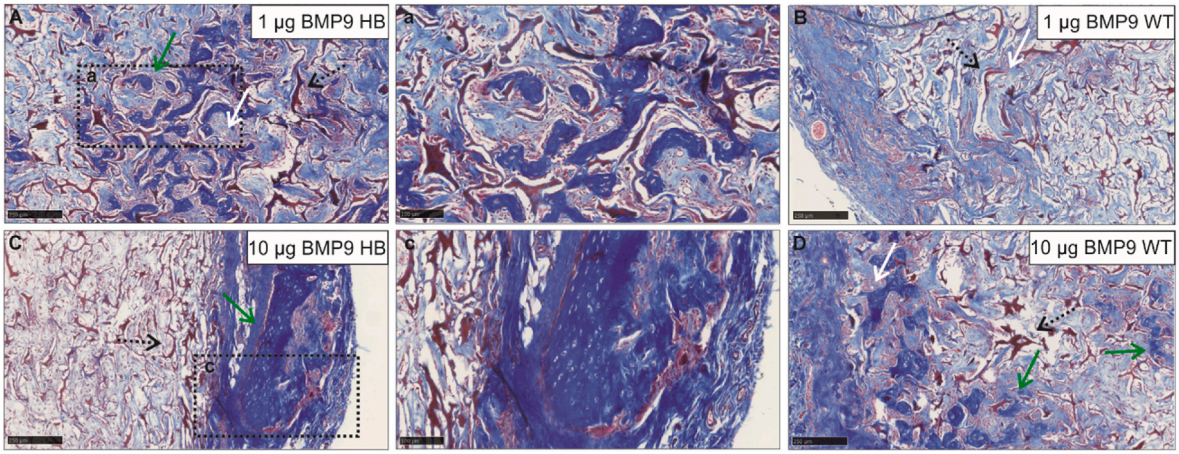


**Fig. 3.** Histological analyses of bone formed 3 weeks post implantation. Representative histological images (Masson's trichrome staining) of implants retrieved 3 weeks post implantation: **A.** and **a.** 1 µg BMP9 HB, **B.** 1 µg BMP9 WT, **C.** and **c.** 10 µg BMP9 HB, **D.** 10 µg BMP9 WT. Scale bar: 250 µm in A, B, C and D and 100 µm in a and c. White arrows indicate blood vessel, black arrows with dashed line show remnants of collagen scaffold, green arrows indicate newly formed bone which is also shown at a higher magnification in a and c.

the ligand (Fig. 5 F and G).The BMP2 WT-loaded scaffold created bone with a more uniformly distributed structure (Fig. 5H). However, the BMP2 WT-induced bone seems to be in a more premature stage of bone formation compared to that induced byBMP9 HB, which instead seems to reflect later stages. Histological examination of the collagen scaffold implanted without any growth factor did not show bone formation (Suppl. Table 2).

## 3. Discussion

Here we demonstrate that genetically engineering BMP9 by introducing features of BMP2 results in a growth factor that can induce the formation of mineralized bone tissue in an ectopic model at a lower concentration than either BMP2 WT or BMP9 WT. Thus, the combination of two features, the strong osteogenic potential of BMP9 as demonstrated *in vitro* by inducing alkaline phosphatase expression in e.g., C2C12 cells and a stronger retention in tissue provided by the introduced heparin binding sites resulted in a BMP9 HB ligand with a strong osteogenic activity *in vivo*. Ectopic bone formation induced by BMP9 HB appears at 10-fold lower doses if compared to the commonly used BMP2 WT.

The produced BMP9 HB contains the receptor binding epitopes (the so-called wrist- or knuckle epitopes) of BMP9. In SPR measurements, almost identical sensorgrams could be recorded for the interaction of BMP9 and BMP9 HB with either the type-I receptor ALK1 or the type-II receptor BMPR-II indicating that the binding parameters are not affected by the introduced heparin binding sites present in BMP9 HB. It thus can be concluded that concerning receptor binding capabilities both variants have identical biological activity In contrast, clear differences in activity were observed in cell-based assays; BMP9 HB induced half maximal ALP activity at ligand concentration approximately 3-fold higher than BMP9 WT. Importantly, both BMP9 ligands induced ALP activity much stronger than BMP2 which is considered to be the most potent osteoinductive growth factor for bone generation *in vivo*. The lower *in vitro* activity of BMP9 HB compared to BMP9 WT is most-likely caused by binding of BMP9 HB to structures of the ECM. This implies a lower active concentration of the "free" ligand *ipso facto* resulting in a virtually lower bioactivity. An analogous effect was observed previously for a BMP2 variant (coreBMP2) in which the heparin binding site containing N-terminus was proteolytically cleaved resulting in a decrease of the $EC_{50}$ value of ALP in C2C12 cells [31]. In another BMP2 variant the insertion of additional heparin binding sites into the N-terminus of BMP2 ("T4 BMP2") resulted in a decrease of the osteogenic potential *in vitro* most-likely due to the stronger matrix binding properties of this variant [39]. This T4 BMP2 variant, though, *in vivo* had a better bone forming capability when implanted intra-muscularly into rat hind limbs than BMP2 WT. This discrepancy between *in vitro* and *in vivo* assays was also seen in our experiments comparing BMP9 HB to BMP9 WT; BMP9 HB more potently induced bone formation *in vivo* than BMP9 WT. In summary, the presence of heparin binding sites seems to modulate the osteogenic potential of BMP9, and it appears that heparin-binding capacities inversely correlate with the osteogenic potential of the ligand *in vitro* but correlate positively with its osteogenic potential *in vivo*.

In contrast to BMP2, a single intramuscular injection of rhBMP9 failed to induce heterotopic ossification, which, due to the lack of heparin binding sites, most-likely resulting from higher diffusion rates of BMP9 [40]. Instead, rhBMP9-adsorbed scaffolds have been shown to be able to induce bone formation in ectopic or calvaria defect models [30]. We also found bone formation with the highest dose of BMP9 in our ectopic bone formation model, comparable to that observed with the highest dose of BMP2. However, although BMP2 WT and BMP9 WT showed no or little bone formation at a dose of 1 µg, BMP9 HB induced significant amounts of bone tissue, in terms of both, bone volume and density in all samples. Interestingly, even the lowest dose of BMP9 HB, 0.1 µg, showed osteopromotive potential, supporting the efficacy of the combination of BMP2-derived heparin binding motifs with the stimulatory capacity provided by BMP9 being further enhanced by the ligand's Noggin-insensitivity.

Striking differences in the structure of the formed bone were apparent when comparing bone formation of the two heparin binding site-containing proteins, BMP2 WT and BMP9 HB. With 1 µg of BMP9 HB, all the implants induced bone formation with a structure resembling a long bone with the cortical part and the central bone marrow. Instead, with 1 µg BMP2 WT only small clusters of bone tissue were formed but the result was not consistent within the different implants. While with 10 µg BMP9 HB, bone formation is triggered from the periphery with the bone formation mainly on the outside probably impeding the infiltration of bone-forming cells into the inner region. This effect appears to a lesser extent in the case of BMP2 WT, where the newly formed bone is more similar to trabecular bone. BMP9 HB induces a bone like structure already at the low dose of 1 µg whereas the other proteins fail to induce bone formation.

BMP9 signals through the type I receptor ALK1, typically expressed in endothelial cells, but also through ALK2, which is also utilized by BMP6 and 7, strongly suggesting that the mechanisms governing BMP9-mediated osteoinduction may differ from BMP2 that uses the BMP type I receptor BMPR-IA (ALK3) that is known to be expressed differentially in various tissues [41]. Since bone repair occurs *in vivo* in a vascularized

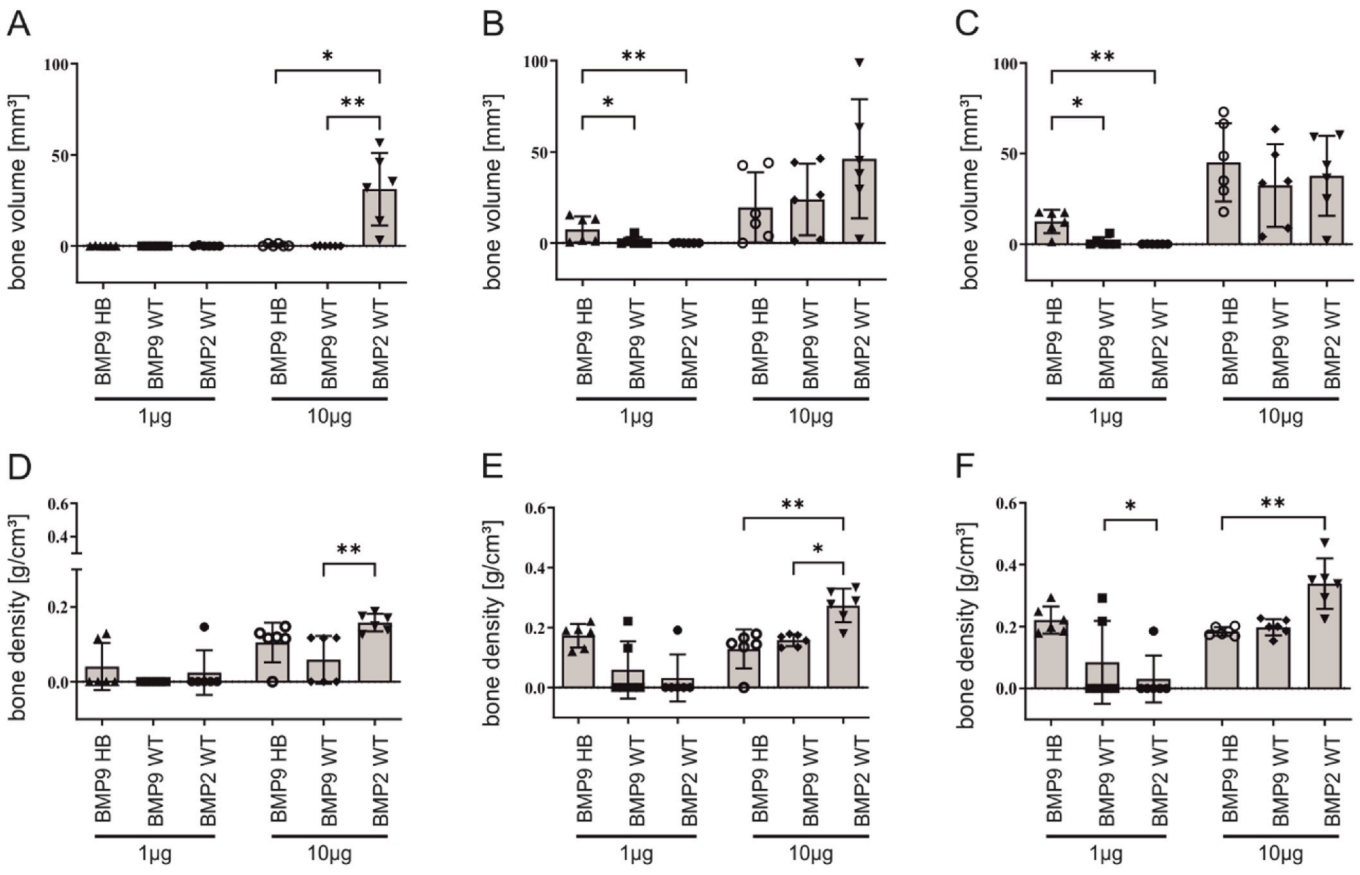


| | BMP9 HB | | BMP9 WT | | BMP2 WT | |
|---|---|---|---|---|---|---|
| | 1 μg | 10μg | 1 μg | 10μg | 1 μg | 10μg |
| 3 weeks | 2 | 5 | 0 | 3 | 1 | 6 |
| 6 weeks | 6 | 5 | 2 | 6 | 1 | 6 |
| 8 weeks | 6 | 6 | 2 | 6 | 1 | 6 |

**Fig. 4.** Longitudinal evaluation of bone volume (BV) and bone mineral density (BMD). (A, B, C) Comparison of the mineral volume obtained in the different conditions at 3 (A), 6 (B), and 8 (C) weeks-periods by longitudinal imaging. (D, E, F) Comparison of bone mineral density at 3 weeks (D), 6 weeks (E) and 8 weeks (F). All the animals are included in the graphs (also values equal to 0). The table below the graph shows the number of subcutaneous mineralized tissues detected (values different from 0 were counted as detected bone) over a $n = 6$. Data represent mean values ± Standard Deviation. Statistical analyses were performed by one-way ANOVA by Dunn's multiple comparisons test.

environment, several osteogenic precursors might be attracted via the invading capillaries and then differentiate towards bone forming cells. These could be pericytes which have been demonstrated to be capable of differentiating into an osteogenic lineage [42], but also vascular smooth muscle cells (VMSC) [43] and muscle resident stromal cells (mrSCs) [40] have demonstrated BMP9-dependent osteogenic differentiation. Moreover, BMP9 could be involved in the process of epithelial to mesenchymal transition (EMT) [44,45]. Since the produced BMP9 HB variant has the same binding affinities to the same receptors of BMP9 WT, it would attract cells from the same lineage and drive them towards osteogenic differentiation. It is remarkable, that BMP9 HB is able to induce bone formation stronger than the well-known BMP2 in a subcutaneous environment like in our animal study and future studies could provide information about which cells participate in BMP9-driven bone formation.

Taken together, our results strongly suggest a yet unexplored potential of BMP9 made more potent in case of our engineered version of BMP9 HB for the treatment of bone defects. As BMP9 knockout mice do not display any compromised bone phenotype it can be suggested that native BMP9 obviously does not play an important role in the development and maintenance of bone tissue. BMP9 can, however, be converted into a powerful osteogenic growth factor simply by adding heparin-binding properties. The introduction of these binding-sites allows a proper fixation of the ligand to suitable materials and the longer retention of the modified factor at the implant site supports the formation of newly formed bone. Notably, the lower BMP9 HB doses required to achieve significant formation of new bone might open new strategies for growth factor enforced treatment of bone defects.

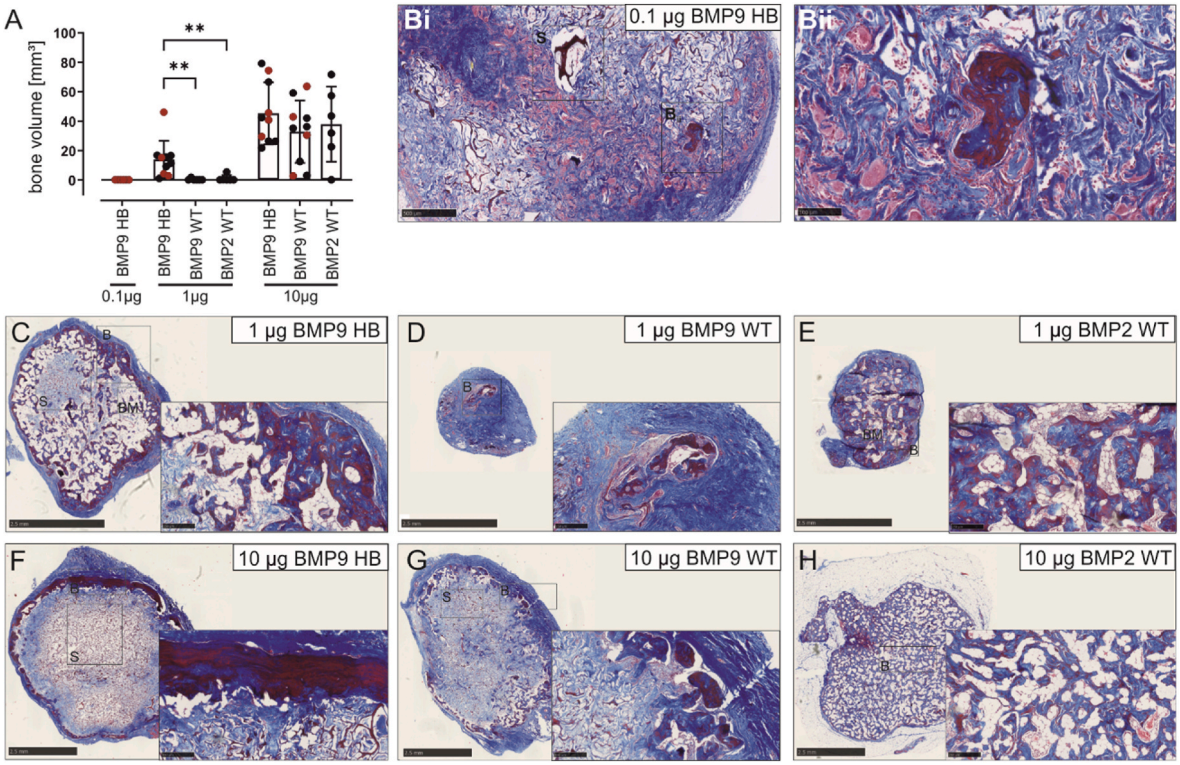


**Fig. 5.** Evaluation of bone volume (BV) and histological examination of the implants retrieved 8 weeks post implantation. (A) The bone volume of the retrieved ossicles at 8 weeks is shown as bar diagram. Black symbols represent retrieved implants from the first batch of animals and red symbols represent the ones from the second batch ($n = 6$ for the conditions: 0.1 μg BMP9 HB, 1 μg BMP2 WT, 1 μg BMP9 WT, 10 μg BMP2 WT. $n = 10$ for the conditions: 1 μg BMP9 HB, 10 μg BMP9 WT and 10 μg BMP9 HB). Data represent mean values ± Standard Deviation. Statistical analyses were performed by one-way ANOVA by Dunn's multiple comparisons test, $p < 0.01$. (B–H) Representative Masson's trichrome-stained sections of implants at 8 weeks. ($B_i$ and $B_{ii}$) 0.1 μg BMP9 HB, (C, D and E) 1 μg of BMP9 HB, BMP9 WT, BMP2 WT and (F, G and H) 10 μg BMP9 HB, BMP9 WT, BMP2 WT loaded collagen scaffold. Traces of the collagen scaffold (S), bone tissue (B) and fatty bone marrow (BM) are indicated. Scale bars in C, D, E and F, G, H: 2.5 mm. Scale bars in $B_i$ 500 μm and in all the enlargements in C, D, E, F, G, H: 250 μm. Scale bar in $B_{ii}$ 100 μm.

## 4. Materials and methods

### 4.1. Construction and purification of BMP9 HB

BMP9 HB was generated by combining the N-terminal segment encoding sequence of BMP2 WT with the cysteine-knot motif encoding sequence of BMP9 WT by recombinant PCR resulting in the mature part encoding amino acid sequence MAQAHKHQRKRLKSS*CQKT SLRVNFE-DIGWD-SWIIAPKEYEAYECKGGCFFPLADDVTPT-KHAIVQTLVHLKFPTKVGKACCVPTKLSPISVLYKDDMGVPTLKY-HYEGMSVAECGCR* (BMP2 = plain; BMP9 = italic). The PCR product encoding BMP9 HB was subsequently cloned into *Nco*I and *Bam*HI restriction sites of the expression vector pQKa, a commercially available vector backbone (pQE, Qiagen, Hilden, Germany) in which the ampicillin resistance gene (β-Lactamase) has been replaced by sequence that encodes for kanamycin resistance. DNA sequences of positive clones were verified by DNA-sequencing.

*Protein expression and purification.* A single colony was inoculated overnight in Lysogeny Broth (LB) and propagated further in Terrific Broth (TB). At optical density of 600 nm ($OD_{600}$) = 0.8 the cultures were induced by adding Isopropyl β-D-1-thiogalactopyranoside (IPTG) to a concentration of 1 mM. Detailed protocols for BMPs expression, inclusion body extraction and protein purification are detailed described in Refs. [13,32].

*SDS Gel Electrophoresis and Coomassie Brilliant Blue staining.* 5 μg of CHO-cell derived BMP9 WT (provided by Peprotech, Cranbury, NJ, USA), or BMP9 HB were separated by SDS-PAGE either under reducing or non-reducing conditions and subsequently stained with Coomassie Brilliant Blue R-250 (Thermo Fisher Scientific).

*Glycoprotein staining.* The different proteins, 10 μg of horseradish peroxidase serving as positive control, 10 μg of soybean trypsin inhibitor as negative control and 5 μg of either BMP9 WT or BMP9 HB were subjected to SDS-PAGE. The control proteins were applied under reducing while BMP9 WT and BMP9 HB were loaded using non-reducing conditions. After electrophoresis potential glycosylation was analyzed using the Pierce® Glycoprotein Staining Kit (ThermoFisher Scientific, Waltham, MA, USA) according to the supplier's recommendations.

*Alkaline phosphatase assay.* The ALP assays were performed using the myoblastic cell line C2C12 (ATCC CRL-172) as previously described [46]. Cells were exposed to increasing concentrations of BMP2 WT (*E. coli* derived; produced in house [31]), BMP9 WT or BMP9 HB. Ligand-induced ALP expression was analyzed after 72 h of incubation. ALP activity was determined by spectrophotometric analysis of 4(para)--nitrophenyl-phosphate (pNPP) conversion at a wavelength of 405 nm using a Tecan Infinite M200 reader (Tecan, Maennedorf, Kanton Zuerich, Switzerland). Dose-response curves were generated using the software OriginPro9.1. ALP assays including the modulator protein Noggin (provided by Peprotech, Cranbury, NJ, USA)) were performed using the different ligands at their individual calculated $EC_{50}$ values (BMP9 WT: 0.87 nM, BMP9 HB: 2.4 nM BMP2 WT: 22 nM) which were premixed with Noggin to a final concentration of 50 nM. As control, ligands were applied at the above mentioned concentration without Noggin.

*Surface Plasmon Resonance:* A Reichert4SPR surface plasmon resonance system (Reichert Technologies) was used for all surface plasmon resonance measurements. Measurements with immobilized receptor ectodomains were performed at 25 °C using 10 mM HEPES pH 7.4, 500 mM NaCl, 3.4 mM EDTA, and 0.005% (v/v) Tween-20 as running buffer.

The flow rate for interaction data acquisition was set to 10 μl/min. Measurements with the immobilized human $ALK1_{ECD}$ were recorded at a flow rate of 25 μL/min using the same running buffer. The monomeric receptor ectodomains of human BMPR-IA (amino acids 24 to 152), human BMPR-II (amino acids 32 to 150) and human ALK1 (amino acids 22 to 118) were expressed with a C-terminal thrombin cleavage site (LVPRGS) followed by a His6-tag in baculoviral infected Sf9 insect cells as detailed described previously [31,47]. For the interaction analysis of BMP2 WT, BMP9 WT and BMP9 HB with the extracellular domains of human ALK1, human BMPR-IA and human BMPR-II the receptor ectodomains (ECDs) were biotinylated at a 1:1 molar stoichiometric ratio using Sulfo–NHS–LC-biotin (Pierce, Thermo Fisher Scientific) according to the manufacturer's recommendations.

A CMD200 biosensor chip (Xantec Bioanalytics GmbH) was first activated using EDC/NHS according to manufacturer's recommendation, then streptavidin was perfused over the activated sensor surface at a concentration of 100 μg/mL thus immobilizing streptavidin corresponding to 2000 to 2500 resonance units (RU) per channel. The biotinylated receptor ectodomains were subsequently immobilized to the prepared streptavidin sensor surface at a density of approximately 350–500 RU. For binding kinetic analyses, different analyte concentrations in the range of 1 - 200nMwere used. The association time was set to 360 s in case of measurements with immobilized human $BMPR\text{-}IA_{ECD}$ and human $BMPR\text{-}II_{ECD}$ and to 180 s in case of measurements employing human $ALK1_{ECD}$. Data for dissociation rate constants were generally obtained by perfusing the sensor chip surface with running buffer for 180 s. After each ligand perfusion, the sensor chip was regenerated by perfusing 6 M Urea/Acetic acid, pH 3 for 20 s. To remove bulk-face effects (buffer jumps, etc.) and unspecific binding of the proteins to the sensor chip matrix the interaction of the analyte to the unmodified streptavidin surface (empty channel 4) was subtracted from all sensorgrams. Binding affinities were calculated by fitting the association and dissociation phase of the sensorgrams using a grouped regression analysis of the rate constants and employing 1:1 Langmuir type interaction model (global fit). Standard deviations of equilibrium binding constants are calculated from two independent experiments using at least four different analyte concentrations. Interactions between the investigated ligands and immobilized Noggin (provided by Peprotech, Cranbury, NJ, USA) were recorded similarly. For these measurements biotinylated recombinant Noggin was immobilized to the Streptavidin functionalized chip surface at a density of approximately 100 RU. Association and dissociation times were each set to 180 s at 25 °C and a flow rate of 25 μL/min using the same running buffer mentioned before.

For the interaction analyses of BMP2 WT, coreBMP2 (a BMP2 WT variant where the N-terminal-heparin binding site segment was enzymatically cleaved [31]), BMP9 WT and BMP9 HB with heparin a HC200 M chip (Xantec Bioanalytics GmbH) was used. Using the afore mentioned protocol the chip surface was activated with EDC/NHS but here neutravidin was perfused over the activated sensor surface at a concentration of 100 μg/mL thus immobilizing neutravidin corresponding to 5000 to 7000 resonance units (RU) per channel. Heparin (Carl Roth GmbH, Karlsruhe, Germany) with a molecular weight of ~20.000 g/mol was biotinylated at a 1:40 molar stoichiometric ratio using Sulfo–NHS–LC-biotin (Pierce, Thermo Fisher Scientific) according to the manufacturer's recommendations. The biotinylated heparin was immobilized to the prepared neutravidin sensor surface at a density of approximately 1800 RU. For binding kinetic analyses, different analyte concentrations in the range of 1–200 nM were used. Sensorgrams were recorded at 25 °C and a flow rate of 25 μL/min using 10 mM HEPES pH 7.4, 150 mM NaCl, 3.4 mM EDTA, and 0.005% (v/v) Tween-20 as running buffer. Times for association and dissociation phases were set to 180s.

### 4.2. Preparation and characterization of the collagen scaffold

The scaffold was obtained by a standardized process, starting with an aqueous solution of atelocollagen (1% w/w) in acetic acid dissolved in double-distilled water after setting the pH to 5.5 by adding 0.1 M NaOH. The precipitate is homogenized by moderate stirring and rinsed in distilled water. To stabilize the scaffold and slow down its degradation kinetics in an *in vivo* physiological environment, the fibrous structures were chemically cross-linked by a 16-h treatment at room temperature in 1 wt% 1,4-butanediol di-glycidyl ether bis-epoxy carbonate (BDDGE) buffer. After chemical cross-linking, the fibers were filtered and the entire scaffold was freeze-dried with controlled freezing and heating ramps, resulting in a three-dimensional composite scaffold. Finally, it is gamma sterilized at 25 KGray.

The morphology and microstructure of the collagen scaffolds were analyzed by Scanning Electron Microscopy (SEM) (Cambridge LEO 438 VP). Samples were observed in partial vacuum to avoid pretreatment and the need for metallization.

#### 4.2.1. In vitro release of BMP2 WT, BMP9 WT and BMP9 HB from the collagen scaffold

Collagen scaffolds (d = 10 mm and h = 4 mm) were placed in a 12 well-plate and soaked with 10 μg of either BMP2 WT, BMP9 WT or BMP9 HB (150 μL, 66.6 μg/mL) for 30 min at room temperature. After allowing the scaffolds to absorb the solution, 2 mL of alpha MEM (Gibco) with 1.5 μg/mL amphotericin B (Fungizone) (Invitrogen) and 50 μg/mL gentamicin (Gibco) were added, and plates were incubated at 37 °C. At each time point medium supernatants were completely removed, collected, and subsequently replaced by the same volume of fresh medium. The release of BMP2 WT, BMP9 WT and BMP9 HB was determined for 7 days. As positive controls, 5 μg/mL of each protein was incubated for the same time in alpha MEM with 1.5 μg/mL fungizone and 50 μg/mL gentamicin. At every time point 100 μL of the control solutions were sampled. The controls were included to calculate the protein portion released at each time point by correcting for loss by adsorbance to the tube and/or degradation of the proteins. The samples were analyzed by either using the BMP-2 Standard ABTS ELISA development kit (Peprotech) or by the duoset BMP9 ELISA kit (R&D) for both BMP9 and BMP9 HB. Before starting the experiment, the detection accuracy of the BMP9 ELISA kit was validated for BMP9 HB. Both proteins, BMP9 WT and BMP9 HB were equally detected.

### 4.3. In vivo studies

All animal experiments were performed with prior approval of the Erasmus MC ethics committee for laboratory animal use (project number: AVD101002015114 and protocol number: 15-114-07).

For the subcutaneous ectopic bone formation model, a total of 14 14-week-old male Sprague Dawley (SD) rats (Charles River) were used in this study. The animals were randomly assigned and housed in pairs in specific-pathogen-free conditions and allowed to adapt to the conditions of the animal facility for 7 days before implantation. To ensure pre- and post-operative analgesia, 1 h before surgery and 6–8 h after surgery rats received 0.05 mg/kg bodyweight of buprenorphine subcutaneously (Temgesic, Reckitt Bensicker). Collagen scaffolds (d = 10 mm and h = 4 mm) were soaked for 30 min before implantation with 150 μL saline containing either one of the following protein doses: 1 μg BMP2 WT, 10 μg BMP2 WT, 1 μg BMP9 WT, 10 μg BMP9 WT, 0.1 μg BMP9 HB, 1 μg BMP9 HB and 10 μg BMP9 HB. An overview of the distribution of the different conditions is shown in Suppl. Fig. 5. For the negative controls, scaffolds were loaded with 150 μL of saline solution.

Animals were anesthetized with isoflurane inhalation (4% to induce, 2.5% to maintain). The incision area was shaved and disinfected. During surgery, 5 or 6 transverse incisions were made in the dorsal skin and subcutaneous pockets were created by blunt dissection. The scaffolds were implanted in the pockets (1 scaffold per pocket, 5–6 scaffolds per animal) and the incisions were closed by polylactic acid sutures (Vycril 4.0, Ethicon). Animals were allowed to recover and were closely monitored over the subsequent days for any signs of distress, discomfort,

or infection. The animals were maintained at 22 ± 5 °C on a 12 h dark/light cycle with access to standard rat chow and water ad libitum. All the operated animals were included in the study. Exclusion criteria were set a priori and included a body-weight reduction of 20%. The first part of the experiment aimed to understand BMP9 HB and BMP9 WT early ectopic bone formation. Therefore, animals with 1 μg and 10 μg BMP9 HB or 1 μg and 10 μg BMP9 WT were euthanized 3 weeks after surgery and samples processed for histology. In the second part of the study, we aimed to observe bone formation after 8 weeks. In this case all the above conditions were tested: 0.1 μg ($n = 6$), 1 μg and 10 μg BMP9 HB ($n = 10$), 1 μg BMP9 WT ($n = 6$) and 10 μg BMP9 WT ($n = 10$) and 1 μg and 10 μg BMP2 WT ($n = 6$). The animals were euthanized 3- or 8-weeks post implantation and samples processed for histology. Blinding was possible during outcome assessment and data analysis.

### 4.4. Micro-computed tomography (micro-CT) analysis

To investigate bone mineralization kinetics, a Quantum GX micro-CT (PerkinElmer, Waltham, MA, USA) was used every 2–3 weeks until the end of the experiment. Time points for the first batch of animals of conditions 1 μg and 10 μg BMP2 WT, BMP9 WT and BMP9 HB, $n = 6$ for all conditions, were 3, 6, and 8 weeks post implantation. Additional animals were included in the groups: 1 μg and 10 μg BMP9 HB and 10 μg BMP9 WT ($n = 4$) and an additional group was included in the second batch of animals with 0.1 μg BMP9 HB ($n = 6$). These animals were only scanned after 8 weeks *ex vivo* since this animal study was ongoing during COVID-lockdown restrictions. It was therefore not possible to access the animal facility to perform micro-CT scanning at week 3 and 6 post implantation, respectively. To image bone formation *in vivo* the following parameters were used: Acquisition: 86, Recon: 86 (pixel size: 172 μm), Scan Time: 4 min, Voltage: 90 kV and Current: 88 μA. Instead for the *ex vivo* these parameters were used: Acquisition: 72, Recon: 45 (pixel size: 90 μm), Scan Time: 4 min, Voltage: 90 kV and Current: 88 μA.

Bone volume (BV) and bone mineral density (BMD) were measured based on calibration scanning using two phantoms with known density (0.25 and 0.75 g/cm$^3$; Bruker Micro-CT) under identical conditions. For image processing, the Analyze 11 software was used (Mayoclinic, Rochester, MN, USA), and threshold levels were set to 0.12 g/cm$^3$.

### 4.5. Histological analysis of explanted implants

For histological analyses, 3 and 8 weeks after subcutaneous implantation in rats, samples were removed and fixed in neutral buffered 4% formalin solution for at least 72 h. Then, samples were decalcified in 10% ethylenediaminetetraacetic acid (EDTA) for 3 weeks and embedded in paraffin. Sections of 6 μm thickness were collected along the long axis of the cylindrical samples on a saw Microtome system (Leica 4 RM2235, Germany). Three cross sections, at least 200 μm apart from each other, were collected from each sample. The sections were deparaffinized and rinsed with distilled water and stained afterwards with hematoxylin and eosin (H&E) and with Masson's trichome.

### 4.6. Statistical analysis

Data were analyzed using the IBM Statistics 21 (SPSS) and GraphPad software (GraphPad, San Diego, USA). Data of BMP release were analyzed using a Kolmogorov-Smirnov's test. *In vivo* data were analyzed using two-way analysis of variance. If the overall differences were significant, differences between groups were analyzed by Bonferroni post hoc test. A value of $p < 0.05$ was considered statistically significant.

## 5. One sentence summary

The addition of heparin binding sites to BMP9 wild type (WT) creates a more potent osteogenic protein compared to BMP2 WT or BMP9 WT *in vivo*.

## Funding

The research leading to these results has received funding from the European Union Seventh Framework Programme FP7-PEOPLE-2013-ITN under grant agreement no. 607051 in project BioInspire, the Netherlands Organisation of Scientific Research – Applied and Engineering Science under the frame of EuroNanoMed III in project NanoScores (project nr ENMIII077-2) and by the University of Wuerzburg (funding program OpenAccess Publishing).

## Author contributions

C.S. and S.F.G performed and planned the experiments, performed the data analysis, elaborated the figures and drafted the manuscript; V.N prepared the BMP9 HB variant; N.K. performed the histology, L.D and M.M.M. prepared the collagen scaffold and performed the analyses, Y.R. performed the micro CT; E.F. participated in the animal study design; G. J.V.M.V.O. was involved in the project and designed and supervised the animal study; J.N. designed the BMP9 HB variant, performed the SPR experiments, designed and organized the project. All the authors agreed on the content of the manuscript. Main inputs and contributions for the manuscript writing and revision were given from S.C., S.F.G., E.F., G.J. V.M.V.O., J.N.

## Data availability

All data associated with this study are present in the paper or Supplementary Materials.

## Ethics approval

All animal experiments were performed with prior approval of the Erasmus MC ethics committee for laboratory animal use (project number: AVD101002015114 and protocol number: 15-114-07).

## Declaration of competing interest

All authors declare, that no conflict of interest exists.

## Acknowledgments

The authors would like to thank the staff of the Erasmus MC in Rotterdam for the professional support during the animal study. Collagen scaffold was provided by Finceramica. This work was supported through the use of imaging equipment provided by the Applied Molecular Imaging Erasmus MC facility.

## Appendix A. Supplementary data

Supplementary data to this article can be found online at https://doi.org/10.1016/j.bioactmat.2023.07.010.

## References

[1] M.R. Urist, Bone: formation by autoinduction, Science 150 (3698) (1965) 893–899.
[2] W.F. McKay, S.M. Peckham, J.M. Badura, A comprehensive clinical review of recombinant human bone morphogenetic protein-2 (INFUSE Bone Graft), Int. Orthop. 31 (6) (2007) 729–734.
[3] J.W. Hustedt, D.J. Blizzard, The controversy surrounding bone morphogenetic proteins in the spine: a review of current research, Yale J. Biol. Med. 87 (4) (2014) 549–561.
[4] J.K. Burkus, M.F. Gornet, C.A. Dickman, T.A. Zdeblick, Anterior lumbar interbody fusion using rhBMP-2 with tapered interbody cages, J. Spinal Disord. Tech. 15 (5) (2002) 337–349.
[5] P.J. Boyne, R.E. Marx, M. Nevins, G. Triplett, E. Lazaro, L.C. Lilly, M. Alder, P. Nummikoski, A feasibility study evaluating rhBMP-2/absorbable collagen sponge for maxillary sinus floor augmentation, Int. J. Periodontics Restor. Dent. 17 (1) (1997) 11–25.

[6] R. Vaidya, J. Carp, A. Sethi, S. Bartol, J. Craig, C.M. Les, Complications of anterior cervical discectomy and fusion using recombinant human bone morphogenetic protein-2, Eur. Spine J. 16 (8) (2007) 1257–1265.

[7] L.B. Shields, G.H. Raque, S.D. Glassman, M. Campbell, T. Vitaz, J. Harpring, C. B. Shields, Adverse effects associated with high-dose recombinant human bone morphogenetic protein-2 use in anterior cervical spine fusion, Spine (Phila Pa 31 (5) (1976) 542–547, 2006.

[8] A.W. James, G. LaChaud, J. Shen, G. Asatrian, V. Nguyen, X. Zhang, K. Ting, C. Soo, A review of the clinical side effects of bone morphogenetic protein-2, Tissue Eng. B Rev. 22 (4) (2016) 284–297.

[9] D. Mumcuoglu, C. Siverino, B. Tabisz, B. Kluijtmans, J. Nickel, How to use BMP-2 for clinical applications? A review on pros and cons of existing delivery strategies, J. Trans. Sci. 3 (5) (2017) 1–11.

[10] K. Kashiwagi, T. Tsuji, K. Shiba, Directional BMP-2 for functionalization of titanium surfaces, Biomaterials 30 (6) (2009) 1166–1175.

[11] K. Yuasa, E. Kokubu, K. Kokubun, K. Matsuzaka, K. Shiba, K. Kashiwagi, T. Inoue, An artificial fusion protein between bone morphogenetic protein 2 and titanium-binding peptide is functional in vivo, J. Biomed. Mater. Res. 102 (4) (2014) 1180–1186.

[12] Y. Zhao, J. Zhang, X. Wang, B. Chen, Z. Xiao, C. Shi, Z. Wei, X. Hou, Q. Wang, J. Dai, The osteogenic effect of bone morphogenetic protein-2 on the collagen scaffold conjugated with antibodies, J. Contr. Release 141 (1) (2010) 30–37.

[13] C. Siverino, B. Tabisz, T. Luhmann, L. Meinel, T. Muller, H. Walles, J. Nickel, Site-directed immobilization of bone morphogenetic protein 2 to solid surfaces by click chemistry, J. Vis. Exp. 133 (2018).

[14] C. Siverino, S. Fahmy-Garcia, D. Mumcuoglu, H. Oberwinkler, M. Muehlemann, T. Mueller, E. Farrell, G. van Osch, J. Nickel, Site-directed immobilization of an engineered bone morphogenetic protein 2 (BMP2) variant to collagen-based microspheres induces bone formation in vivo, Int. J. Mol. Sci. 23 (7) (2022).

[15] K.K. Wurzler, J. Emmert, F. Eichelsbacher, N.R. Kubler, W. Sebald, J.F. Reuther, [Evaluation of the osteoinductive potential of genetically modified BMP-2 variants], Mund-, Kiefer- Gesichtschirurgie 8 (2) (2004) 83–92.

[16] R. Depprich, J. Handschel, W. Sebald, N.R. Kubler, K.K. Wurzler, [Comparison of the osteogenic activity of bone morphogenetic protein (BMP) mutants], Mund-, Kiefer- Gesichtschirurgie 9 (6) (2005) 363–368.

[17] L. Macri, D. Silverstein, R.A. Clark, Growth factor binding to the pericellular matrix and its importance in tissue engineering, Adv. Drug Deliv. Rev. 59 (13) (2007) 1366–1381.

[18] H. Cheng, W. Jiang, F.M. Phillips, R.C. Haydon, Y. Peng, L. Zhou, H.H. Luu, N. An, B. Breyer, P. Vanichakarn, J.P. Szatkowski, J.Y. Park, T.C. He, Osteogenic activity of the fourteen types of human bone morphogenetic proteins (BMPs), J Bone Joint Surg Am 85 (8) (2003) 1544–1552.

[19] Q. Kang, M.H. Sun, H. Cheng, Y. Peng, A.G. Montag, A.T. Deyrup, W. Jiang, H. H. Luu, J. Luo, J.P. Szatkowski, P. Vanichakarn, J.Y. Park, Y. Li, R.C. Haydon, T. C. He, Characterization of the distinct orthotopic bone-forming activity of 14 BMPs using recombinant adenovirus-mediated gene delivery, Gene Ther. 11 (17) (2004) 1312–1320.

[20] J.J. Song, A.J. Celeste, F.M. Kong, R.L. Jirtle, V. Rosen, R.S. Thies, Bone morphogenetic protein-9 binds to liver cells and stimulates proliferation, Endocrinology 136 (10) (1995) 4293–4297.

[21] J.D. Lamplot, J. Qin, G. Nan, J. Wang, X. Liu, L. Yin, J. Tomal, R. Li, W. Shui, H. Zhang, S.H. Kim, W. Zhang, J. Zhang, Y. Kong, S. Denduluri, M.R. Rogers, A. Pratt, R.C. Haydon, H.H. Luu, J. Angeles, L.L. Shi, T.C. He, BMP9 signaling in stem cell differentiation and osteogenesis, Am J Stem Cells 2 (1) (2013) 1–21.

[22] J. Luo, M. Tang, J. Huang, B.C. He, J.L. Gao, L. Chen, G.W. Zuo, W. Zhang, Q. Luo, Q. Shi, B.Q. Zhang, Y. Bi, X. Luo, W. Jiang, Y. Su, J. Shen, S.H. Kim, E. Huang, Y. Gao, J.Z. Zhou, K. Yang, H.H. Luu, X. Pan, R.C. Haydon, Z.L. Deng, T.C. He, TGFbeta/BMP type I receptors ALK1 and ALK2 are essential for BMP9-induced osteogenic signaling in mesenchymal stem cells, J. Biol. Chem. 285 (38) (2010) 29588–29598.

[23] S.H. McBride-Gagyi, J.A. McKenzie, E.G. Buettmann, M.J. Gardner, M.J. Silva, Bmp2 conditional knockout in osteoblasts and endothelial cells does not impair bone formation after injury or mechanical loading in adult mice, Bone 81 (2015) 533–543.

[24] G.Q. Zhao, Consequences of knocking out BMP signaling in the mouse, Genesis 35 (1) (2003) 43–56.

[25] N. Ricard, D. Ciais, S. Levet, M. Subileau, C. Mallet, T.A. Zimmers, S.J. Lee, M. Bidart, J.J. Feige, S. Bailly, BMP9 and BMP10 are critical for postnatal retinal vascular remodeling, Blood 119 (25) (2012) 6162–6171.

[26] P. Mahlawat, U. Ilangovan, T. Biswas, L.Z. Sun, A.P. Hinck, Structure of the Alk1 extracellular domain and characterization of its bone morphogenetic protein (BMP) binding properties, Biochemistry 51 (32) (2012) 6328–6341.

[27] S.A. Townson, E. Martinez-Hackert, C. Greppi, P. Lowden, D. Sako, J. Liu, J. A. Ucran, K. Liharska, K.W. Underwood, J. Seehra, R. Kumar, A.V. Grinberg, Specificity and structure of a high affinity activin receptor-like kinase 1 (ALK1) signaling complex, J. Biol. Chem. 287 (33) (2012) 27313–27325.

[28] M.A. Brown, Q. Zhao, K.A. Baker, C. Naik, C. Chen, L. Pukac, M. Singh, T. Tsareva, Y. Parice, A. Mahoney, V. Roschke, I. Sanyal, S. Choe, Crystal structure of BMP-9 and functional interactions with pro-region and receptors, J. Biol. Chem. 280 (26) (2005) 25111–25118.

[29] T. Nakamura, Y. Shirakata, Y. Shinohara, R.J. Miron, K. Furue, K. Noguchi, Osteogenic potential of recombinant human bone morphogenetic protein-9/absorbable collagen sponge (rhBMP-9/ACS) in rat critical size calvarial defects, Clin. Oral Invest. 21 (5) (2017) 1659–1665.

[30] M. Fujioka-Kobayashi, M.A. El Raouf, N. Saulacic, E. Kobayashi, Y. Zhang, B. Schaller, R.J. Miron, Superior bone-inducing potential of rhBMP9 compared to rhBMP2, J. Biomed. Mater. Res. 107 (6) (2019) 1351.

[31] K. Heinecke, A. Seher, W. Schmitz, T.D. Mueller, W. Sebald, J. Nickel, Receptor oligomerization and beyond: a case study in bone morphogenetic proteins, BMC Biol. 7 (2009) 59.

[32] M.M. Kuo, P.H. Nguyen, Y.H. Jeon, S. Kim, S.M. Yoon, S. Choe, MB109 as bioactive human bone morphogenetic protein-9 refolded and purified from E. coli inclusion bodies, Microb. Cell Factories 13 (1) (2014) 29.

[33] J. Nickel, W. Sebald, J.C. Groppe, T.D. Mueller, Intricacies of BMP receptor assembly, Cytokine Growth Factor Rev. 20 (5–6) (2009) 367–377.

[34] C. Chang, Agonists and antagonists of TGF-beta family ligands, Cold Spring Harbor Perspect. Biol. 8 (8) (2016).

[35] A. Bharadwaz, A.C. Jayasuriya, Osteogenic differentiation cues of the bone morphogenetic protein-9 (BMP-9) and its recent advances in bone tissue regeneration, Mater Sci Eng C Mater Biol Appl 120 (2021), 111748.

[36] S. Keller, J. Nickel, J.L. Zhang, W. Sebald, T.D. Mueller, Molecular recognition of BMP-2 and BMP receptor IA, Nat. Struct. Mol. Biol. 11 (5) (2004) 481–488.

[37] S. Fahmy-Garcia, D. Mumcuoglu, L. de Miguel, V. Dieleman, J. Witte-Bouma, B.C. J. van der Eerden, M. van Driel, D. Eglin, J.A.N. Verhaar, S. Kluijtmans, G. van Osch, E. Farrell, Novel in situ gelling hydrogels loaded with recombinant collagen peptide microspheres as a slow-release system induce ectopic bone formation, Adv Healthc Mater 7 (21) (2018), e1800507.

[38] D. Mumcuoglu, S. Fahmy-Garcia, Y. Ridwan, J. Nicke, E. Farrell, S.G. Kluijtmans, G.J. van Osch, Injectable BMP-2 delivery system based on collagen-derived microspheres and alginate induced bone formation in a time- and dose-dependent manner, Eur. Cell. Mater. 35 (2018) 242–254.

[39] R. Ruppert, E. Hoffmann, W. Sebald, Human bone morphogenetic protein 2 contains a heparin-binding site which modifies its biological activity, Eur. J. Biochem. 237 (1) (1996) 295–302.

[40] E. Leblanc, F. Trensz, S. Haroun, G. Drouin, E. Bergeron, C.M. Penton, F. Montanaro, S. Roux, N. Faucheux, G. Grenier, BMP-9-induced muscle heterotopic ossification requires changes to the skeletal muscle microenvironment, J. Bone Miner. Res. 26 (6) (2011) 1166–1177.

[41] D. Chen, M. Zhao, G.R. Mundy, Bone morphogenetic proteins, Growth Factors 22 (4) (2004) 233–241.

[42] M.J. Doherty, B.A. Ashton, S. Walsh, J.N. Beresford, M.E. Grant, A.E. Canfield, Vascular pericytes express osteogenic potential in vitro and in vivo, J. Bone Miner. Res. 13 (5) (1998) 828–838.

[43] D. Zhu, N.C. Mackenzie, C.M. Shanahan, R.C. Shroff, C. Farquharson, V.E. MacRae, BMP-9 regulates the osteoblastic differentiation and calcification of vascular smooth muscle cells through an ALK1 mediated pathway, J. Cell Mol. Med. 19 (1) (2015) 165–174.

[44] Q. Li, X. Gu, H. Weng, S. Ghafoory, Y. Liu, T. Feng, J. Dzieran, L. Li, I. Ilkavets, M. Kruithof-de Julio, S. Munker, A. Marx, A. Piiper, E. Augusto Alonso, N. Gretz, C. Gao, S. Wolfl, S. Dooley, K. Breitkopf-Heinlein, Bone morphogenetic protein-9 induces epithelial to mesenchymal transition in hepatocellular carcinoma cells, Cancer Sci. 104 (3) (2013) 398–408.

[45] Y. Wang, B. Yang, J. Zhao, X. Yu, X. Liu, L. Zhang, Y. Zhang, X. Li, Z. Zhai, Epithelialmesenchymal transition induced by bone morphogenetic protein 9 hinders cisplatin efficacy in ovarian cancer cells, Mol. Med. Rep. 19 (3) (2019) 1501–1508.

[46] T. Katagiri, A. Yamaguchi, M. Komaki, E. Abe, N. Takahashi, T. Ikeda, V. Rosen, J. M. Wozney, A. Fujisawa-Sehara, T. Suda, Bone morphogenetic protein-2 converts the differentiation pathway of C2C12 myoblasts into the osteoblast lineage, J. Cell Biol. 127 (6 Pt 1) (1994) 1755–1766.

[47] T. Kirsch, J. Nickel, W. Sebald, BMP-2 antagonists emerge from alterations in the low-affinity binding epitope for receptor BMPR-II, EMBO J. 19 (13) (2000) 3314–3324.